Proceedings of the 30th International Cosmic Ray Conference
Rogelio Caballero, Juan Carlos D'Olivo, Gustavo Medina-Tanco,
Lukas Nellen, Federico A. Sánchez, José F. Valdés-Galicia (eds.)
Universidad Nacional Autónoma de México,
Mexico City, Mexico, 2008
Vol. 1 (SH), pages 853–856

30TH INTERNATIONAL COSMIC RAY CONFERENCE

Anomalous cosmic rays at a blunt termination shock

J. KÓTA
University of Arizona, Lunar and Planetary Laboratory, Tucson, Arizona 85721-0092 USA
kota@lpl.arizona.edu

Abstract: We present numerical simulations modeling acceleration of ACR around a blunt termination shock with the spiral field lines intersecting the shock multiple times. The 2-D model includes parallel and perpendicular diffusion. Our results confirm the qualitative expectations: the nose segment of the blunt shock is inefficient to accelerate particles to ACR energies, which results in a continuing increase of the ACR flux and a gradual unfolding of the ACR spectrum behind the shock, as seen by Voyager-1. We also present a simple analytically tractable testcase to illustrate physical effects at a 2-D shock with structure along the shockfront.

Introduction

The ACR spectrum did not fully unfold but remained modulated when Voyager-1 (V-1) reached the termination shock (TS) at the end of 2004, [1],[2]. MeV ACR fluxes continued to increase and the spectrum unfolded eventually as V-1 moved farther into the heliosheath. Earlier, the anti-sunward anisotropies observed upstream indicated [3], [4], [5] that V-1 was on a field line that crossed and re-crossed the shock between V-1 and the Sun. Such multiple intersection should occur due to the bluntness of the TS [6]. Preliminary works also suggested that this same field topology can accelerate only to TSP energies, but is inefficient to accelerate to ACR energies. Hence ACRs, which must be accelarated at farther part of the TS, would not fully unfold when V-1 crosses the shock. McComas and Schwadron [7] suggested that acceleration of ACR occurs toward the flanks of the blunt shock. Temporal rather than spatial dynamical variations have been offered as alternative explanation [8] In this work we consider a blunt shock with multiple intersection and present numerical simulations considering Parker's equation, including shock acceleration and anisotropic diffusion ($\kappa_{\|}$, $\kappa_{\perp}$).

The schematic cartoon of Figure 1 illustrates an example of multiple intersection that results in three (or more) intersections with the TS. Shock acceleration occurs at all three intersections S1, S2, and S3. ACR energies are reached, however, only at the rightmost intersection (S1), where enough time is available for acceleration. At the "new" sites (S2 and S3) acceleration starts only when the field line hits the shock. Low-energy particles from S2 and S3 could be seen since V-1 was is close to these sites (nose). Higher energy ACRs, however, are accelerated at farther segment of the TS, hence ACRs remain modulated. For a blunt shock [7], the basic principles are the same; the nose direction would correspond to the region between S3 and S2.

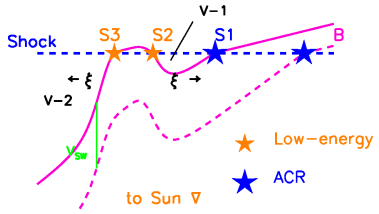

Figure 1: Schematic cartoon (not in scale) illustrating multiple intersections (S1, S2, S3) between the mean magnetic field and the shock The new, 'fresh' sites $S3$ $S2$ cannot accelerate to high energies since time is insufficient (see text).

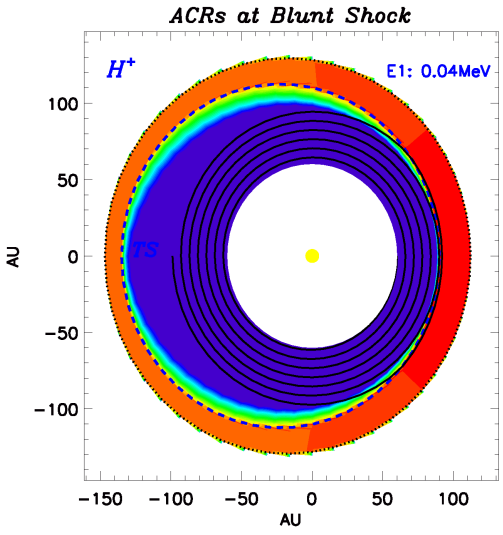

Figure 2: Distribution of simulated 40 keV TSPs around the blunt TS (dashed line).

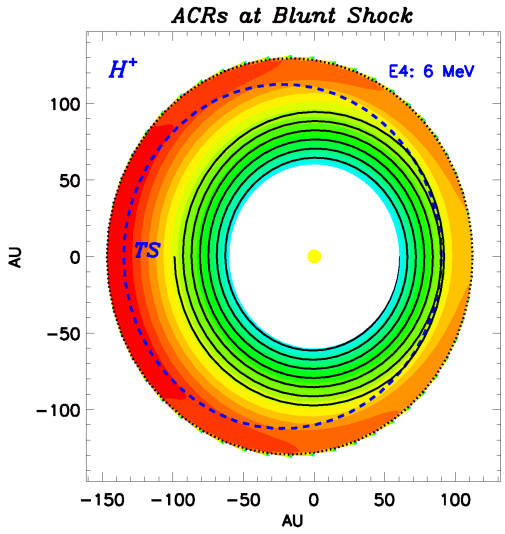

Figure 3: Simulated 6 MeV ACR fluxes around the blunt TS. Note the nose/tail asymmetry.

Modelling ACRs at a blunt termination shock

In the simulations presented here, we consider a conceptually simple 2-D case, neglecting drift and latitudinal motion but capturing the essential longitudinal structure. The TS represented by an offset circle is intersected by the spiral field multiple times. Beside the field-aligned parallel diffusion we also include perpendicular diffusion, taking $\kappa_{perp}/\kappa_{\parallel}$ 0.02. A 10 keV seed population proportional to r^{-2} is injected at the TS.

At low energies (Figure 2) acceleration is fast and occurs locally, which yields a largely uniform TSP distribution everywhere along the shock. Toward higher energies, however, acceleration at nose turns out ineffective, which results in lower ACR flux at the nose segment of the TS (Figure 3). The 6 MeV ACR flux continues to increase well into the inner heliosheath. This is also clearly seen in Figure 4, which shows the radial variation of particle fluxes (at five different energies) at the longitude of V-1.

Shown in Figure 5 is the energy spectrum along the shock. In the nose region (red) ACRs remain modulated at the shock while a harder unfolded spec-

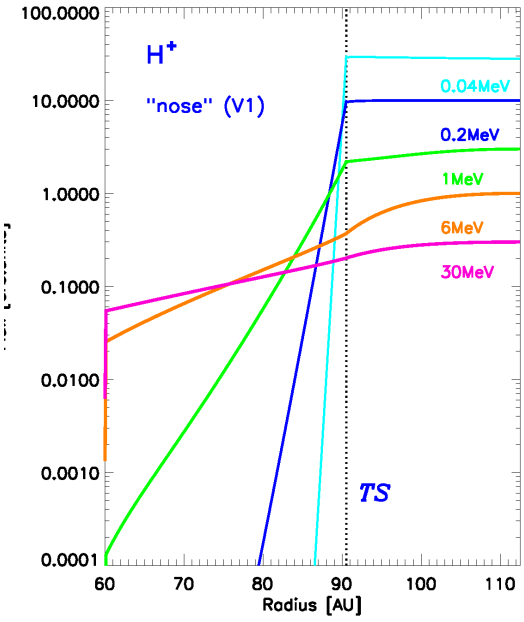

Figure 4: Radial variation of fluxes of various particle energies along the longitude of Voyager-1. MeV fluxes continue to increase and reach maximum behind the TS.

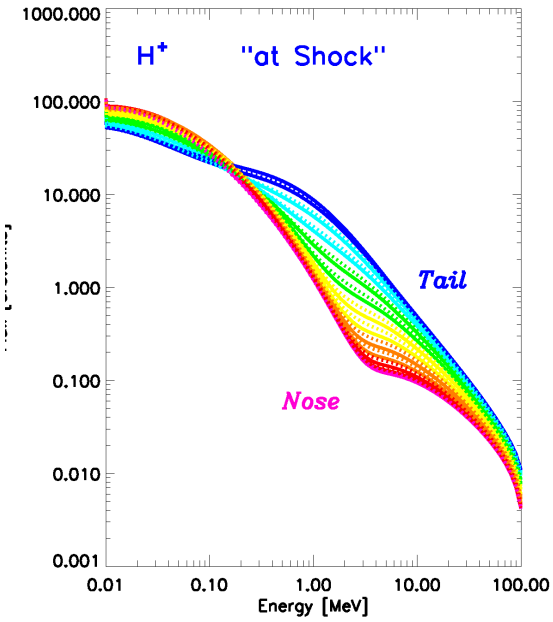

Figure 5: Variation of the energy spectrum along the blunt TS. The modulated spectrum at the nose (red) gradually unfolds toward the tail (blue)

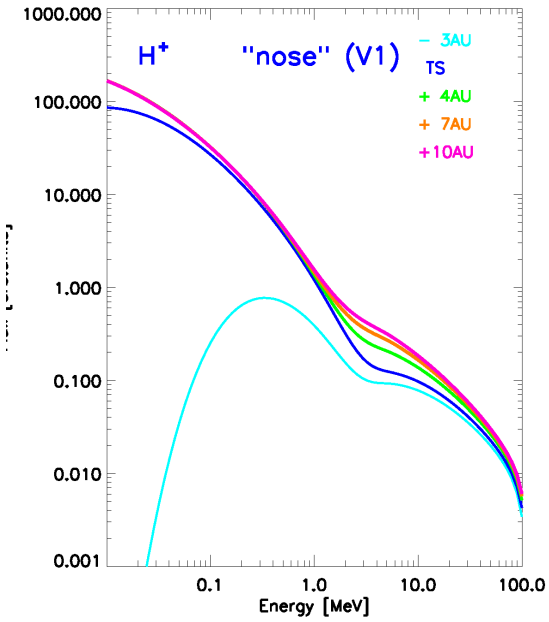

Figure 6: Predicted spectrum for V-1 at different distances into the heliosheath.

trum is expected toward the flanks and tail. Figure 6 showing the spectrum at different distances from the TS illustrates how the ACR spectrum seen by V-1 is predicted to unfold behind the shock.

Predictions for Voyager-2, which are not shown here, turn out qualitatively quite similar to those for Voyager-1, with exception that the direction of the anisotropy is opposite for the two s/c. It should be kept in mind, however, that the offset of the nose direction resulting from the distortion due to the local interstellar magnetic field may well be different for the northern and southern hemispheres.

Finally, we note that, in this simulation, perpendicular diffusion is small ($\kappa_\perp/\kappa_\parallel = 0.02$). A larger $\kappa_\perp$ will produce qualitative similar results. Effects associated with the field line topology, which are quite pronounced here, will be smaller but remain still significant. More quantitative works are in progress. At energies above ~10MeV, latitudinal motion becomes increasingly important, calling for 3-D modeling.

Simple 2-D shock example

Figures 7 and 8 illustrate the effects that can be expected at a 2-D shock with longitudinal structure. In tis section, we consider a simple, analytically tractable case with the magnetic field changing direction along the shock. Assuming periodic boundary condition the scenario resembles to the blunt TS, the places where the field first/last hits the shock correspond to the nose/tail directions. At low energies, close to the injection energy, acceleration occurs locally resulting in a largely uniform distribution along the shock (Fig 7). At higher energies, however, the distribution tends toward

$$f \propto (\frac{p_0}{p})^{3r/(r-1)} \times exp \int V_i \kappa_{ij}^{-1} dx_j \quad (1)$$

which may exhibit a remarkable longitudinal structure (Fig 8) with a longitudinal gradient of

$$\frac{\partial ln\, f}{\partial y} = \frac{V}{\kappa_\perp} (1 - \kappa_\perp/\kappa_\parallel)\, sin\Theta_{Bn} \cos\Theta_{Bn} \quad (2)$$

Behind the shock, diffusion along the field lines relaxes the longitudinal gradient and the longitudi-

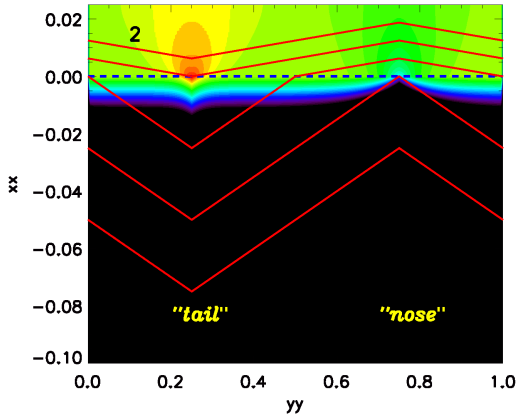

Figure 7: Particle fluxes at a 2-D shock at low energy (twice the injection speed, $\kappa_\perp/\kappa_\parallel = 0.01$)

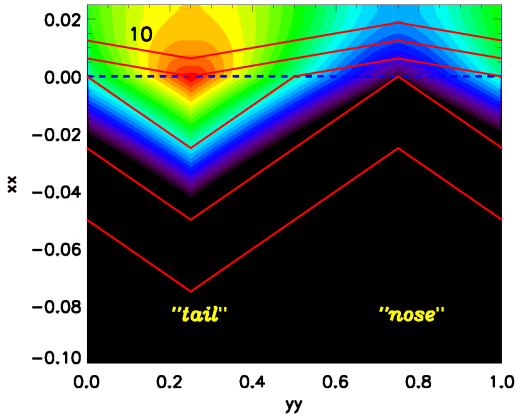

Figure 8: Same as Figure 7, but at higher energies (10 times injection speed)

nal distribution eventually becomes more uniform. Maximum is reached well behind the shock in the 'nose' region. The spectrum starts as a power low everywhere, but it becomes steeper in the nose region, and less steep in the tail region as the spatial distribution adjust to the one described by (1). At still higher energies, the longitudinal variation decreases as the diffusion tensor, κ increases.

We note that (1) would be an analytical solution is the diffusion tensor, κ, were rigidity independent, and diffusion were negligible ($\kappa = 0$) in the downstream region.

Conclusions

We considered a 2-D model neglecting drift and latitudinal motion but capturing the longitudinal structure with magnetic field lines intersecting the blunt TS multiple times. We find that this model may account for V-1 observations both prior to and after the TS crossing. Low-energy particles streaming from the nearby intersection produce large field aligned upstream anisotropies, explaining the precursor events. It also explains why ACR spectrum need not unfolded at the shock crossing in 2004. Acceleration cannot start before the field line hits the shock, hence, time is insufficient for ACR energies. ACRs must be accelerated further away the TS.

We emphasize that a 2-D shock, with a structure along the shock, may not produce a uniform power-law spectrum everywhere. To illustrate this a simple, analytically tractable example was presented. The topology between the shock and field lines may be of importance in other shocks as well.

Acknowledgements

The author benefited from discussions with E.C. Stone, R.B. Decker, J.R. Jokipii, and J Giacalone. This work was supported by NASA under grants NNX07AH19G and LWS04-0029-0003, and by NSF under grant ATM-0330829.

References

[1] Stone, E. C. et al, *Science*, **309**, 2017 (2005).
[2] Decker, R. B. et al, *Science*, **309**, 2020 (2005).
[3] Kóta, J. and J.R. Jokipii, AIP 719, 272–278 (2004).
[4] Jokipii, J.R. et al, *Ap. J.*, **605**, L145 (2004)
[5] Jokipii, J.R. et al, *Ap. J.*, **611**, L141 (2004)
[6] Zank, G.P., *Space Sci. Rev.*, **89**, 413 (1999).
[7] McComas, D. J. and N.A. Schwadron, *Geophys. Res. Lett.*, **33** 25437 (2006).
[8] Florinski, V. and G.P. Zank, *Geophys. Res. Lett*, **33**, L15110 (2005).